

Channel Models for Medical Implant Communication

Kamran Sayrafiyan-Pour · Wen-Bin Yang ·
John Hagedorn · Judith Terrill ·
Kamya Yekeh Yazdandoost · Kiyoshi Hamaguchi

Received: 31 October 2010 / Accepted: 2 November 2010 / Published online: 9 December 2010
© Springer Science+Business Media, LLC (outside the USA) 2010

Abstract Information regarding the propagation media is typically gathered by conducting physical experiments, measuring and processing the corresponding data to obtain channel characteristics. When this propagation media is human body, for example in case of medical implants, then this approach might not be practical. In this paper, an immersive visualization environment is presented, which is used as a scientific instrument that gives us the ability to observe RF propagation from medical implants inside a human body. This virtual environment allows for more natural interaction between experts with different backgrounds, such as engineering and medical sciences. Here, we show how this platform has been used to determine channel models for medical implant communication systems.

Keywords Channel model · Implant communication system · Immersive visualization system · Body area networks

1 Introduction

Body Area Networks (BAN) consist of RF-enabled wearable and implantable sensory nodes for short range reliable communication in or around a human body. This technology is poised to be a promising interdisciplinary technology with novel uses in pervasive information technology. Pacemakers are the oldest and most successful example of implantable medical devices. Among other applications for such devices, we can point to smart pills for precision drug delivery, glucose monitors and eye pressure sensing systems [1–4]. Similarly, wearable sensor nodes offer an attractive set of applications such as medical/physiological monitoring (e.g. electrocardiogram, temperature, respiration, heart rate, blood pressure), disability assistance and human performance management. Integration of BAN with the existing information infrastructure will create a truly pervasive environment for many of these critical applications with great impact on improving the quality of life. Some recent advances in microelectronics indicate that the technology to achieve ultra-small and ultra-low power devices for these applications is within reach [5, 6]. However, numerous regulatory and technical challenges including efficient transceiver design, reliability, biocompatibility, size, cost, energy source, sensing/actuator technology, privacy and security issues still need to be resolved [7, 8].

In 1999, the Federal Communications Commission (FCC) allocated the frequencies in the 402–405 MHz range to be used for Medical Implant Communication Services

K. Sayrafiyan-Pour (✉) · W.-B. Yang · J. Hagedorn · J. Terrill
Information Technology Laboratory, National Institute
of Standards and Technology (NIST), Gaithersburg,
MD, USA
e-mail: ksayrafiyan@nist.gov

W.-B. Yang
e-mail: wyang@nist.gov

J. Hagedorn
e-mail: hagedorn@nist.gov

J. Terrill
e-mail: Judith.terrill@nist.gov

K. Yekeh Yazdandoost · K. Hamaguchi
National Institute of Information and Communications
Technology (NICT), Yokosuka, Japan
e-mail: yazdandoost@nict.go.jp

K. Hamaguchi
e-mail: hamaguti@nict.go.jp

(MICS). This is an ultra-low power, unlicensed mobile radio service for transmitting data in support of diagnostic or therapeutic functions associated with implanted medical devices. The MICS permits individuals and medical practitioners to utilize ultra-low power medical implant devices, such as cardiac pacemakers and defibrillators without causing interference to other users of the electromagnetic radio spectrum. Among primary reasons for selecting these frequencies, one can point to better propagation characteristics for medical implants, reasonable sized antennas and worldwide availability. An international radio standard for MICS will allow patients with implantable devices to obtain necessary care worldwide.

Knowledge of RF propagation for implantable devices will assist RF engineers to optimize physical layer design and therefore, achieve better performance. Such information is typically gathered by conducting physical experiments, measuring and processing the corresponding data to obtain channel characteristics. In case of medical implants, this could be extremely difficult if at all possible. In this paper, we present a sophisticated and innovative 3D virtual reality simulation platform in order to study electromagnetic propagation from medical implants. Communication with an implanted device can be done from any direction inside or outside the body due to various body postures and human motion. Consequently, a true 3D environment is needed to better capture, visualize and understand RF propagation from/to implants. In the following sections, we describe such a platform and show how it was used to extract a simple statistical path loss model for MICS channels.

This paper is organized as follows. Section 2 will describe the immersive 3D platform that we have constructed to study RF propagation from radio implants. The simulated scenarios and description of our approach are provided in Sect. 3. Then, the statistical path loss model is described in Sect. 4, and finally concluding remarks and future plans are expressed in Sect. 5.

2 A 3D Immersive Platform for Medical Implants

Block diagram of our simulation system is shown in Fig. 1. The main components of this system include: a three-dimensional human body model, the propagation engine which is a three-dimensional full-wave electromagnetic field simulator (i.e. HFSS¹), the 3D immersive and visualization platform, and finally an implantable (or body surface antenna).

¹ HFSS is registered trademark of ANSYS Inc. The HFSS has been used in this research to foster understanding. Such identification does not imply recommendation or endorsement by the National Institute of Standards and Technology, nor does it imply that this product is necessarily the best available for the purpose.

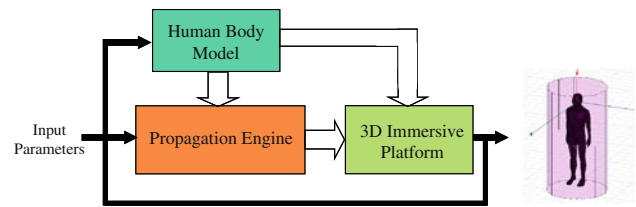


Fig. 1 System block diagram

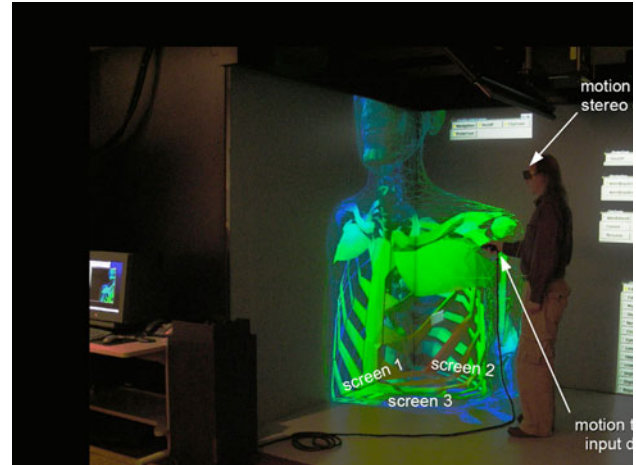


Fig. 2 A user in the NIST immersive visualization environment

The 3D human body model includes frequency dependent dielectric properties of 300+ parts in a male human body. These properties are also user-definable if custom changes or modifications are desired. The human body model has a resolution of 2 mm. The HFSS propagation engine enables us to compute a variety of different electromagnetic quantities such as the magnitude of electric and magnetic fields and Specific Absorption Rate (SAR).

The 3D immersive platform as shown in Fig. 2 includes several important components: three orthogonal screens that provide the visual display, the motion tracked stereo glasses, and the hand-held motion tracked input device. The screens are large projection video displays that are placed edge-to-edge in a corner configuration. These three screens are used to display a single three-dimensional (3D) stereo scene. The scene is updated based on the position of the user as determined by the motion tracker. This allows the system to present to the user a 3D virtual world within which the user can move and interact with the virtual objects. The main interaction device is a hand-held three button motion-tracked wand with a joystick.

This virtual environment allows for more natural interaction between experts with different backgrounds such as engineering and medical sciences. The user can look at data representations at any scale and position, move through data, change orientation, and control the elements

of the virtual world using a variety of interactive measurement and analysis techniques [9]. All of these capabilities are extremely useful when studying RF propagation to/from medical implants.

The final component of our system is the implant antenna. The operating environment for an implant antenna is quite different from the traditional free space communication. Designing an efficient antenna for implantable devices is an essential requirement for reliable MICS operation [10]. The dimension of the antenna must be very small and it should be long term biocompatible [11]. The antenna must also be electrically insulated from the body to avoid possible short circuits [12].

Figures 3 and 4 display the implant antenna used in our simulations. The antenna is composed of a single metallic layer and is printed on a side of a D51 (NTK) substrate with dielectric constant of $\epsilon_r = 30$, loss tangent of $\tan \theta = 0.000038$, and thickness of 1 mm. The metallic layer is copper with 0.036 mm thickness. The dimension of the antenna is $8.2 \times 8.1 \times 1$ mm which is quite appropriate for some medical applications. The metallic layer is covered by RH-5 substrate with dielectric constant of $\epsilon_r = 1.0006$, loss tangent of $\tan \theta = 0$, and thickness of 1 mm. The simulated return loss of this antenna is shown in Fig. 5. Good impedance matching in the MICS frequency band (i.e. 402–405 MHz) is observed. Further details on the design and performance of this antenna can be found in [13, 14].

Input parameters to our system include: antenna position, antenna orientation, operating frequency, transmit power, resolution, range and the choice of the desired

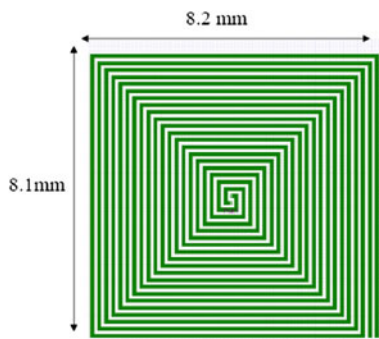


Fig. 3 Front view of the implant antenna

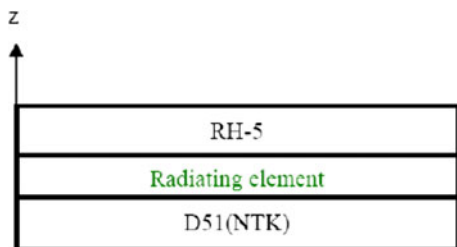


Fig. 4 Side view of the implant antenna

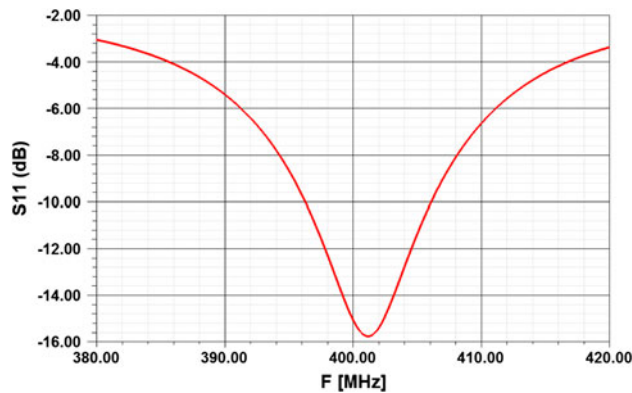


Fig. 5 Return loss of the implant antenna

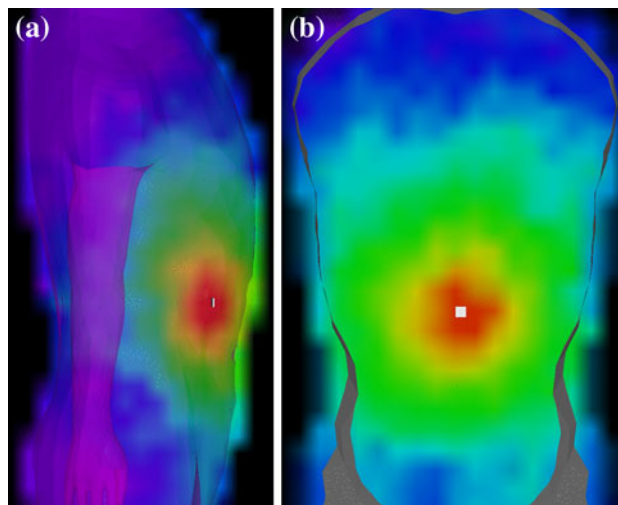


Fig. 6 Sample output image of the immersive system. a Side view. b Front view

output parameters. The operating frequency in this study has been chosen to be 403.5 MHz which is the mid-point of the MICS frequency band. Resolution of 4 mm has been selected to run the simulation and a range (i.e. distance) of 50 cm from the transmitting antenna has been considered.

Figure 6 displays sample output images of our immersive system when an antenna is located in the stomach (e.g. side and front views). The color map shows the signal strength on a 2D plane which is perpendicular (Fig. 6a) or parallel (Fig. 6b) to the antenna plane.

3 Simulation Scenarios

Simulations have been performed for four near-surface implants and two deep-tissue implants applications in a typical male body. The near-surface scenarios include applications such as Implantable Cardioverter-Defibrillator (ICD) and Pacemaker (located below the left pectoral

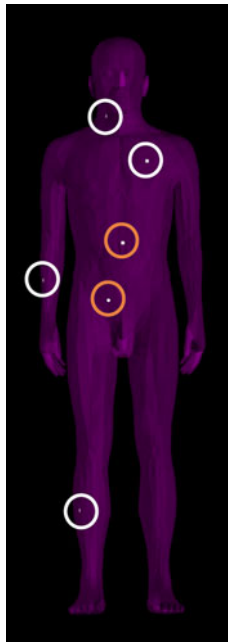


Fig. 7 Various transmitter locations for obtaining signal strength

muscle), Vagus Nerve Stimulation (Right Neck and Shoulder) and two Motion Sensor applications located in right hand and right leg. These locations are highlighted by the white circles in Fig. 7.

The deep tissue implant scenarios considers endoscopy capsule applications for upper stomach (95 mm below body surface) and lower stomach (118 mm below body surface) as highlighted by the red circles in Fig. 7.

For each scenario (i.e. TX location), the received power was calculated for a grid of points within a cylinder area around the body. Then, the resulting data was partitioned into three sets: in-body to in-body, in-body to body surface, and in-body to out-body propagation sets. The in-body to in-body set includes all of the sample points that completely reside inside the body. Likewise, the in-body to body surface set includes all points that reside within a definable distance (i.e. 2 mm, 10 mm, and 20 mm) from the body surface; and finally the in-body to out-body propagation set distinguishes all of the points that reside further away from the body surface.

4 Path Loss Model

Path loss at a distance d from the transmitting antenna, in our calculation, is defined as:

$$PL(d) = \frac{G_R P_T}{P_R(d)}$$

where P_T is the transmit power, P_R denotes the received power and G_R is the receiver antenna gain. Therefore, as

defined in the above equation, the path loss would include the transmitter antenna gain. This is usually not the case for channel models corresponding to most wireless systems, but for MICS, the transmitting antenna is considered to be part of the channel [15]. The path loss in dB at distance d can be statistically modeled by the following equation:

$$PL(d) = PL(d_0) + 10n \log_{10}(d/d_0) + S \quad d \geq d_0$$

where d_0 is the reference distance (i.e. 50 mm), and n is the path loss exponent which heavily depends on the environment where RF signal is propagating through. For, example, it is well known that for free space $n = 2$. Human body is an extremely lossy environment; therefore, much higher value for the path loss exponent is expected. S is the random scatter around the mean and represents deviation in dB caused by different body materials (e.g. bone, muscle, fat, etc.) and the antenna gain in different directions.

We first model the path loss by finding the values for $PL(d_0)$, n and S for deep-tissue versus near-surface implants separately. This will lead to four propagation scenarios i.e. deep-tissue implant-to-implant, near-surface implant-to-implant, deep-tissue implant to body surface and finally near-surface implant to body surface. Next, we combine the deep-tissue and near-surface implant scenarios into one set of data and only consider the propagation channel for the following two cases: implant-to-implant and implant to body surface. This should give us more insight into possible differences between communication channels related to the deep tissue and near surface implants.

Figure 8 shows the scatter plot for the path loss as a function of TX–RX separation for deep tissue implant-to-implant scenarios. The mean value of the random path loss has been displayed by a solid line. This is obtained by

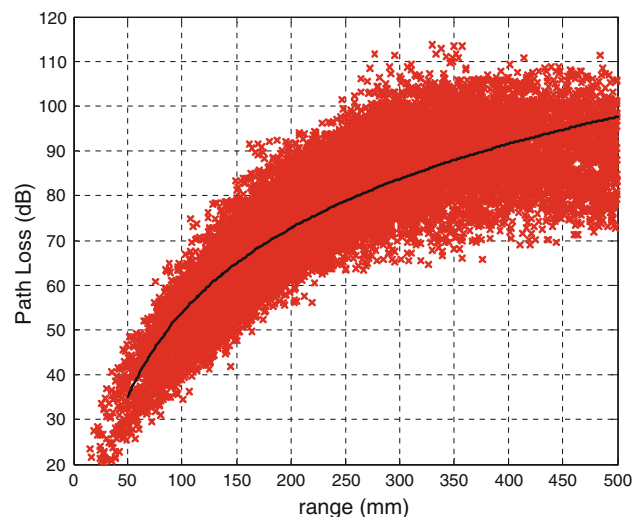


Fig. 8 Scatter plot of the path loss versus distance for deep tissue implant to another implant

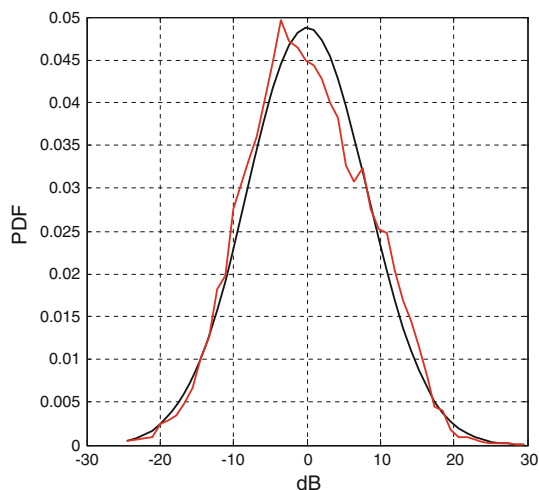


Fig. 9 Distribution of the shadow fading for deep tissue implant to another implant

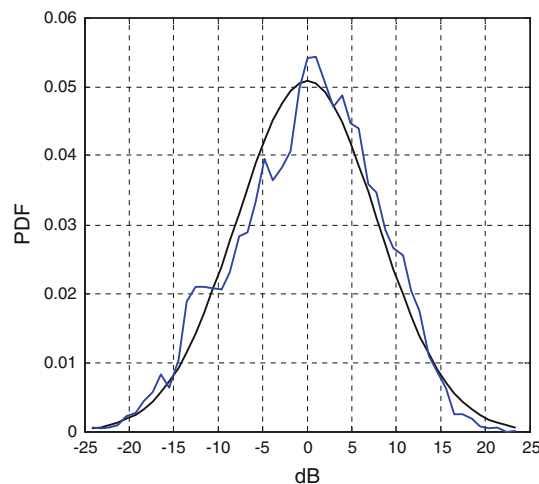


Fig. 11 Distribution of the shadow fading for deep tissue implant to body surface (within 20 mm of the skin)

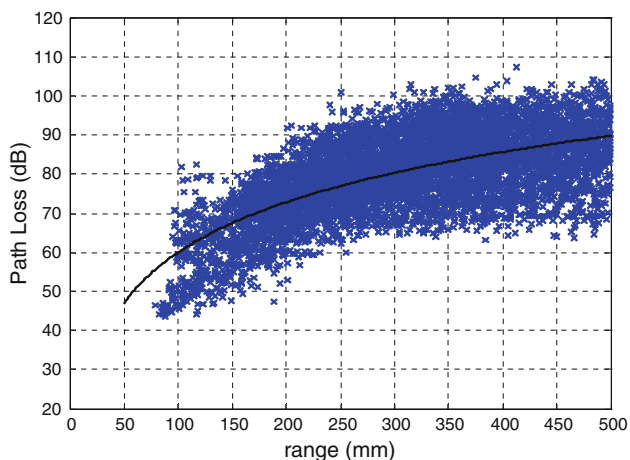


Fig. 10 Scatter plot of the path loss versus distance for deep tissue implant to body surface (within 20 mm of the skin)

fitting a least squares linear regression line through the scatter of measured path loss sample points in dB such that the root mean square deviation of sample points about the regression line is minimized. Random shadowing effects of the channel occur where the TX–RX separation is the same, but have different directions or positions with respect to each other. As shown in Fig. 9, this random variable has a normal distribution with zero mean and standard deviation σ_s , i.e. $S \sim N(0, \sigma_s^2)$.

Similarly, Figs. 10 and 11 represent the path loss scatter plot and probability density function of the shadow fading random variable for the deep tissue implant to body surface scenarios. A distance of up to 20 mm directly from the body surface has been considered in the definition of the body surface sample points. We also tried a separation distance of 2 and 10 mm and observed that the derived path

Table 1 Parameters for the statistical path loss model for the case of deep tissue implant

	PL(d_0) (dB)	n	σ_s (dB)
Deep tissue implant to another implant	35.04	6.26	8.18
Deep tissue implant to body surface	47.14	4.26	7.85

loss parameters did not vary much. One should keep in mind that layers of clothing could cause additional loss to the signal.

Table 1 summarizes the extracted parameters of the statistical path loss models for the above scenarios.

Scatter plots and shadow fading distributions corresponding to the near-surface implant scenarios have been provided in Figs. 12, 13, 14, and 15.

Table 2 summarizes the extracted parameters of the statistical path loss models for the near surface implant scenario.

Deriving a channel model for communication between an implant and another node that resides further away from the body is more challenging. In the simple case of an environment where there are no objects or obstacles, a free space path loss can be added to the above models to account for the additional loss that the implant signal will go through once it leaves the body. On the other hand, if there are objects adjacent to the body in the surrounding environment, further loss could occur and the model needs to be adjusted accordingly. With appropriate assumptions this channel could be considered as an aggregate of two concatenated channels: implant to body surface and body surface to the external node channels. Further analysis and measurement data is needed to investigate this channel and obtain the appropriate statistical models.

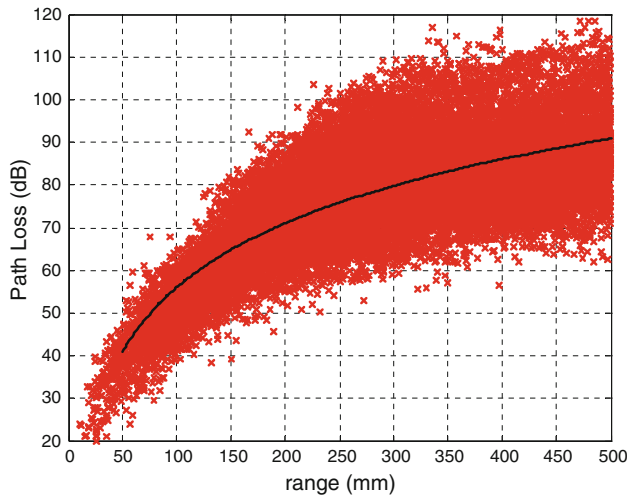


Fig. 12 Scatter plot of the path loss versus distance for near surface implant to another implant

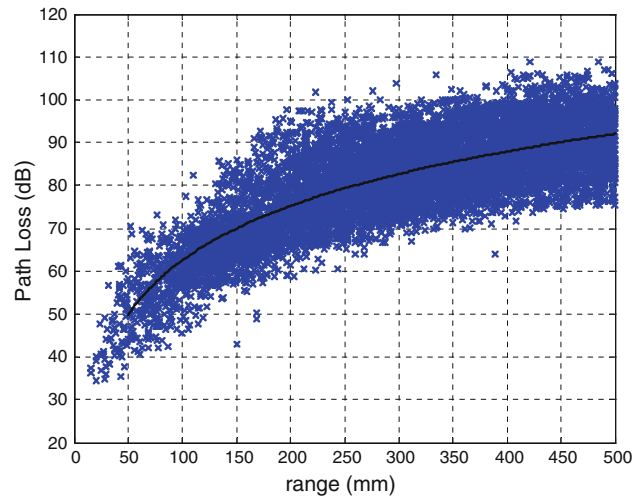


Fig. 14 Scatter plot of the path loss versus distance for near surface implant to body surface (within 20 mm of the skin)

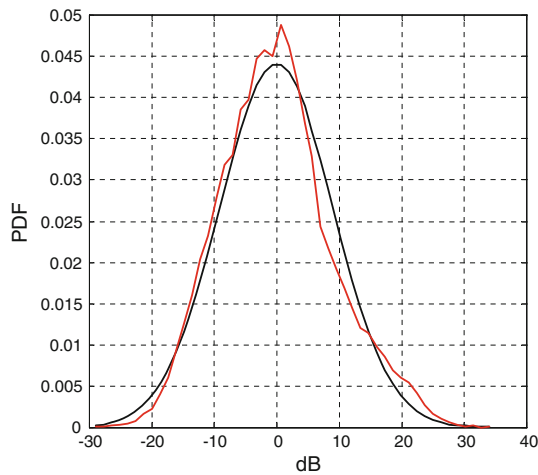


Fig. 13 Distribution of the shadow fading for near surface implant to another implant

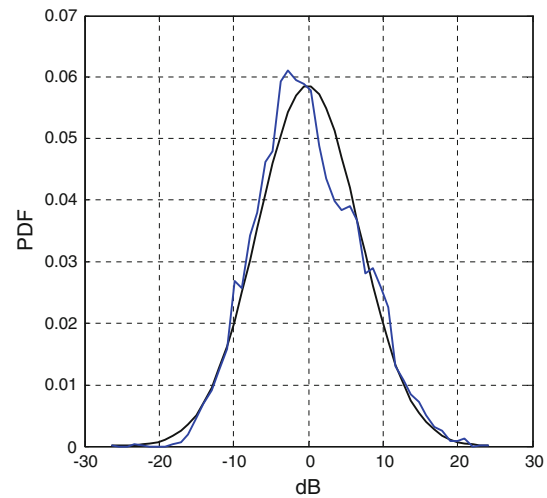


Fig. 15 Distribution of the shadow fading for near surface implant to body surface (within 20 mm of the skin)

5 Conclusion

We have presented an immersive visualization environment to conduct research in order to characterize RF propagation from medical implants. Extensive simulations have been performed to obtain a statistical path loss model for MICS channels. The model is based on four near surface and two deep tissue implant applications in a typical male human body. The authors recognize the fact that the extracted parameters for the statistical model are based on the simulation data; therefore, upon availability of measurement data from physical experiments, the results outlined in this paper should be further validated. However, no such reference data set is currently available. Along this line, efforts are underway to conduct and obtain body surface measurements which can be emulated in the

Table 2 Parameters for the statistical path loss model for the case of near surface implant

	PL(d_0) (dB)	n	σ_s (dB)
Near surface implant to another implant	40.94	4.99	9.05
Near surface implant to body surface	49.81	4.22	6.81

immersive system for cross-verification purposes. The path loss models obtained in this study have been adopted by the IEEE802.15 task group TG6 on body area networks. The accuracy and applicability of such models requires further validation and investigation by scientists and engineers.

In general, studying a specific medical implant application with custom made antennas is also possible with this platform. More in-depth research on this subject is

undoubtedly required to further understand the characteristics of radio frequency propagation from medical implants. The authors hope that the virtual reality environment introduced here would create a flexible platform where more efficient collaboration between engineers and medical experts would become possible.

Acknowledgment The authors would like to thank Mr. Steven Satterfield from the high performance computing and visualization group of the Applied and Computational Mathematics Division, ITL, for his assistance in the system setup and his ongoing contribution in the development of tools for the NIST immersive visualization system.

References

1. B. Chi, J. Yao, S. Han, X. Xie, G. Li, and Z. Wang, Lowpower transceiver analog front-end circuits for bidirectional high data rate wireless telemetry in medical endoscopy applications, *IEEE Transaction Biomedical Engineering*, Vol. 54, No. 7, pp. 1291–1299, 2007.
2. E. H. Sarraf, G. K. Wong, and K. Takahata, Frequency-selectable wireless actuation of hydrogel using micromachined resonant heaters toward implantable drug delivery applications. *Solid-State Sensors, Actuators and Microsystems Conference*, pp. 1525–1528. Denver, CO, USA, 21–25 June 2009.
3. K. H. Shin, C. Y. Moon, T. H. Lee, C. H. Lim, and Y. J. Kim, Implantable flexible wireless pressure sensor module, *Sensors*, 2004, *Proceedings of IEEE Solid-State Sensors, Actuators and Microsystems Conference*, Vol. 2, pp. 844–847. Seoul, Korea, 2004.
4. H. Fassbender, W. Mokwa, M. Gortz, K. Trieu, U. Urban, T. Schmitz-Rode, T. Gottsche, and P. Osypka, Fully implantable blood pressure sensor for hypertonic patients. *IEEE Solid-State Sensors, Actuators and Microsystems Conference*, pp. 1226–1229. IEEE, Piscataway, NJ, 2008.
5. J. L. Bohorquez, A. P. Chandrakasan, and J. L. Dawson, A 350 uW CMOS MSK Transmitter and 400 uW OOK super-regenerative receiver for medical implant communications, *IEEE Journal of Solid-State Circuits*, Vol. 44, No. 4, pp. 1248–1259, 2009.
6. J. Kwong, Y. K. Ramadass, N. Verma, and A. Chandrakasan, A 65 nm Sub-Vt microcontroller with integrated SRAM and switched capacitor DC-DC converter, *IEEE Journal of Solid-State Circuits*, Vol. 44, No. 1, pp. 115–126, 2009.
7. G. Yang, *Body Sensor Networks*, Springer London, 2006. ISBN 1-84628-272-1.
8. W. Yang, K. Sayrafian-Pour, J. Hagedorn, J. Terrill, and K. Y. Yazdandoost, Simulation study of body surface RF propagation for UWB wearable medical sensors. *Proceedings of the 2nd International Symposium on Applied Sciences in Biomedical and Communication Technologies*, ISABEL, 2009.
9. J. G. Hagedorn, J. P. Dunkers, S. G. Satterfield, A. P. Peskin, J. T. Kelso, and J. E. Terrill, Measurement tools for the immersive visualization environment: steps toward the virtual laboratory. *Journal of Research of the National Institute of Standard and Technology*, Vol. 112, No. 5, pp. 257–270, 2007.
10. C. A. Balanis, *Antenna Theory, Analysis and Design*, vol. 2nd, John Wiley & Sons Inc. New York, 1997.
11. C. Polk and E. Postow, *Biological Effects of Electromagnetic Fields*, CRC Press, Inc. Boca Raton, 1996. ISBN 0-8493-0641-8.
12. G. S. Smith, A theoretical and experimental study of the insulated loop antenna in a dissipative medium, *Radio Science*, Vol. 8, pp. 711–725, 1973.
13. K. Y. Yazdandoost and R. Kohno, An antenna for medical implant communication systems. *Proceedings of the 37th European Microwave Conference, Munich, Germany*. Oct. 2007
14. K. Y. Yazdandoost and R. Kohno, Body implanted medical device communications. *IEICE Transactions on Communications*, Vol. E92-B, No. 2, pp. 2741–2749, 2009.
15. P. S. Hall and Y. Hao, *Antennas and Propagation for Body Centric Wireless Communications*, Artech House, Inc. Norwood, MA, 2006. ISBN 1-58053-493-7.

Author Biographies



Kamran Sayrafian-Pour is a program manager at the Information Technology Laboratory of the National Institute of Standards and Technology (NIST) located in Gaithersburg, Maryland. He leads several strategic projects that are focused on Pervasive Computing technologies in Healthcare. He holds Ph.D., M.S. and B.S. degrees in Electrical and Computer Engineering from University of Maryland, Villanova University and Sharif University of Technology, respectively.

Prior to joining NIST, he was the cofounder of Zagros Networks, Inc. a fabless semiconductor company based in Rockville, Maryland where he served as President and senior member of the architecture team. Dr. Sayrafian-Pour is the co-inventor/inventor of four U.S. patents. He is a senior member of IEEE and an adjunct faculty of the University of Maryland. He has served as invited member of technical program committee and co-chair of many international conferences and workshops. His research interests include body area networks, mobile sensor networks and RF-based indoor positioning. He has published over 50 conference and journal papers, and book chapters in these areas. He was the recipient of the IEEE PIMRC 2009 best paper award and has also been recognized as the outstanding faculty of 2010 by the office of advanced engineering education at the University of Maryland, College Park. He has been a contributing member and the co-editor of the channel modeling document of the IEEE802.15.6 international standardization on body area networks.



Wen-Bin Yang received his Ph.D. degree in Electrical Engineering from the University of Maryland at College Park in 1993. Since 2007, he has been with the National Institute of Standards and Technology, where he focuses on body area networks technology. He worked on underwater acoustic communications in the Naval Research Laboratory in Washington DC from 2002 to 2007. His current research interests include wireless communications technology and applications. He was the recipient of the IEEE PIMRC 2009 best paper award.



John Hagedorn received his B.A. and M.S. degrees in Mathematics from the University of Virginia in 1975 and Rutgers University in 1980 respectively. He has worked in the area of scientific computing at Cornell University, NASA, and Circuit Studios. He is currently at the Information Technology laboratory of the National Institute of Standards and Technology working in a variety of technical areas including scientific visualization

and high performance computing. He was the recipient of the IEEE PIMRC 2009 best paper award.



Judith Terrill is a Computer Scientist and the Leader of the high performance computing and visualization group of the Applied and Computational Mathematics Division of the Information Technology Laboratory at NIST. Her research interests include machine discovery in scientific data, quantitative scientific visualization, and parallelization of complex computational codes. She was the recipient of the IEEE PIMRC 2009 best paper award.



Kamya Yekhe Yazdandoost received his Ph.D. degree from University of Pune, India, in 2000. He joined the Communications Research Laboratory (CRL), Japan in 2003 (now, National Institute of Information and Communications Technology: NICT), and has been engaged in research on Ultra WideBand (UWB) and Wireless Body Area Network (BAN) technology. He is currently working as an Expert Researcher at the Medical-ICT

group, National Institute of Information and Communications

Technology, Japan. He is an adjunct Professor at University of Oulu, Finland and he is the recipient of Finland Distinguished Professor Program (FIDIPRO) for the periods of 2010–2014. He was invited Guest Professor at the Asian Institute of Technology in Bangkok Thailand Feb. 2007. He is the Chair of the channel modeling committee of the IEEE.802.15.6 on Body Area Network Standardization and he is a life member of the IEEE Microwave Theory and Techniques Society. He is a representative of the NICT to the European COST2100 Action (Management Committee Meeting on Pervasive Mobile and Ambient Wireless Communications). He is also a Member of European Microwave Association. He is holding four patents and his six other patents are pending. He is also Associate Editor of International Journal of Microwave Science and Technology. He has been the TPC member and session chair of various international conferences. He was the recipient of the IEEE PIMRC 2009 best paper award.



Kiyoshi Hamaguchi received the B.S. and M.S. degrees in electrical engineering from Science University of Tokyo in 1989 and 1991, respectively. He also received the Ph.D. degree in electrical engineering from Osaka University in 2000. Since 1993 he has been with the National Institute of Information and Communications Technology (NICT), Japan, where he has been engaged in research and development on wireless telecommunication

systems. From 2002 to 2003, he was a visiting researcher at University of Southampton, U.K. He received the Young Engineer Award from IEICE in 1997, the Young Scientist Award from Ministry of Education, Culture, Sports, Science and Technology of Japan in 2006 and the Radio Achievement Award from the Association of Radio Industries and Businesses (ARIB) in 2010. He is currently a group leader of Medical ICT group in NICT.